Project of a pressure stabilizing closed system for fast boiling experiments

Arlindo T. SOUZA NETTO[1,2], Arthur V. S. OLIVEIRA[3], Michel GRADECK[1], Rogério GONÇALVES DOS SANTOS[2]

[1]Université de Lorraine, CNRS, LEMTA, Nancy F-54000, France
[2]University of Campinas, School of Mechanical Engineering, Energy Department, Campinas, Brazil
[3]University of São Paulo, São Carlos School of Engineering, Mechanical Engineering Department, São Carlos, Brazil
[*]Corresponding author: theodoro1@univ-lorraine.fr

Abstract - With neither the use of pumps (for excessive cost reasons) nor the use of compressed gas (for safety reasons), designing an experimental bench capable of operating at approximately constant pressure during vaporization of liquids in a closed system is challenging. We present in this paper the step-by-step project of an original pressurization solution for closed systems that has the final purpose of performing pool boiling experiments with water, gasoline, and ethanol at pressures up to 80 bar.

Nomenclature

A	area, m^2
P	pressure, bar
D	diameter, m
L	length, m
k	spring stiffness, N/mm
m	mass, kg
$\dot{m}$	mass flux, kg/s
$\dot{q}$	heat flux, W
T	temperature, °C
h_{fg}	heat of vaporization, J/kg
c_p	specific heat capacity, J/kgK
t	time, s
h	heat transfer coefficient, W/m^{2}K
f	function

Greek symbols	
α	pressure tolerance parameter
ρ	density, kg/m^3
Index and exponent	
l	liquid
v	vapor
c	condensation
fc	free convection
0	initial
min	minimum
max	maximum
1	pipeline
2	condenser
sat	saturation
deg	degradation

1. Introduction

The reduction of pollutant emissions and the improvement of cold phase performance of internal combustion engines (ICEs) can be achieved by heating the liquid fuel prior to its injection into the cylinders [1, 2]. Given the short heating time required as well as the power input, this technique results in the occurrence of boiling on the surface of the heater. The fuel heating phenomenon is especially important to be well understood during the phase shortly before the driver starts the engine, when the fuel rail and heater work in a closed system. This is the most critical stage of the project from a safety point of view, once it implies the rapid boiling of a small, closed volume of inflammable liquid. Moreover, the highest emission rates observed throughout the operation of an ICE normally occur during the cold phase [3, 4, 5]. Hence, heating the fuel until a target temperature becomes important to reduce pollutant emissions in this phase. Driven by this motivation, we present here the design of an experimental bench consisting of a closed system representative of a commercial heated fuel rail used in Brazil.

https://doi.org/10.25855/SFT2022-074

The project features a hand-operated pump for initial pressurization and a test section containing the test fluid and operating with a commercial fuel heater. The use of borosilicate glass in the test section, cameras, and adequate lighting make it possible to visualize and film the experiments. A condenser and a spring-piston system were designed externally to the test section as means to decrease the pressure variations during the tests caused by the vaporization of the liquid fuel. One of the major challenges in the modeling is dealing simultaneously with transient boiling and condensation. Simulations of the heating and cooling processes, which are presented in this paper, indicate that the closed system pressure control using these concepts is possible within the required operating ranges. Several parameters' behaviors such as the condensation length, spring displacement, and pressure throughout the experiments were used as the basis for dimensioning the piston diameter, the spring stiffness, and the condenser tube length.

2. Experimental apparatus design

The experimental apparatus consists of a closed boiling chamber representative of a fuel heating system operating in a vehicle fuel rail. It was projected to operate at pressures up to 80 bar and to work with water, ethanol, and gasoline. The test section has a square cross section of 12 mm edge, and its dimensions are displayed in Figure 1.

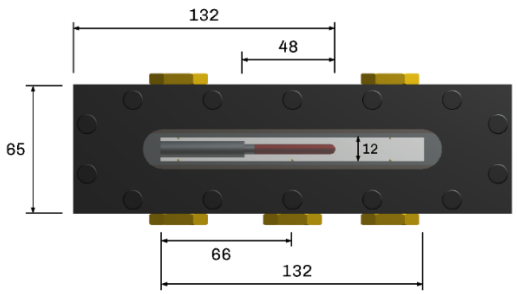

Figure 1: *Front view of the test section (illustrative CAD).*

Figure 2a shows a schematic illustration of the test bench. The pressurization of the system occurs by means of a manual pump (A) associated with the displacement (x) of a piston (B) and consequent compression of a spring (C). A condenser (D) was designed to reduce the pressure variation throughout the experiments due to the generation of vapor by boiling on the surface of the resistive heater (E) positioned inside the test section (F). Table 1 displays the values considered for some variables involved in the project and simulation of the experimental bench.

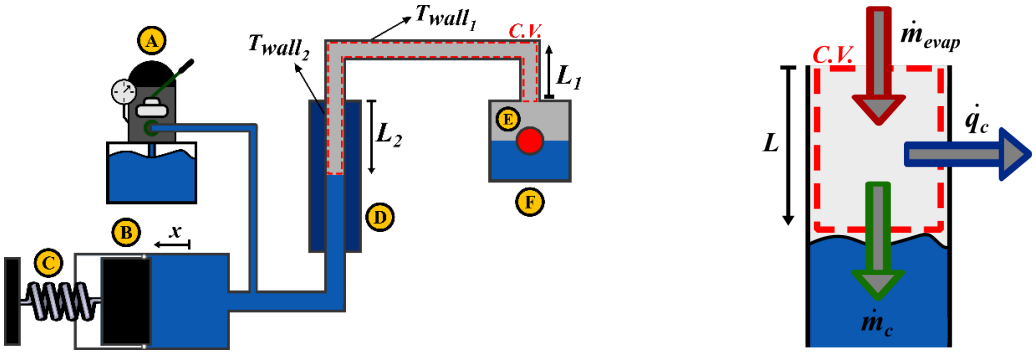

Figure 2: *(a) Schematic drawing of the experimental apparatus, including the (A) manual pump, (B) piston, (C) spring, (D) condenser, (E) resistive heater, and (F) test section. (b) Control volume used for the mass balance analysis.*

Heater power	500 W
Pipeline internal diameter	6 mm
Pipeline external diameter	8 mm
Pipeline length (exposed to air)	200 mm
Condenser internal diameter	6 mm
Condenser external diameter	8 mm
Ambient temperature	20 °C
Temperature of the water in the jacket	20 °C
L_{min} (minimum condensing length)	5 mm
dT_{min} (minimum temperature difference)	1 °C

Table 1: *Characteristics of the experimental bench.*

2.1. Modeling of the pressure control system

Figure 2b displays a control volume (CV) that contains the gas inside the pipeline and condenser tube. The same CV is illustrated in Fig. 2a, where we can notice that there are moments in which condensation occurs only in the pipeline and others in which it occurs both in the latter and in the condenser. In Fig. 2b, $\dot{m}_{evap}$ is the mass flow of steam entering the CV, $\dot{m}_c$ is the mass flow of liquid water leaving the CV after being condensed and $\dot{q}_c$ is the power leaving the CV by condensation on the inner walls of the pipeline ($\dot{q}_{c_1}$) and condenser ($\dot{q}_{c_2}$), when such is the case. A mass balance for this CV can be analyzed to estimate the condensing length behavior during the experiments. The pipeline is externally exposed to ambient air and the condenser consists of a tube surrounded by a water jacket at ambient temperature (20°C). The inner and outer diameters are displayed in Table 1.

The following assumptions have been made with the objective of estimating the variables conservatively and ensuring proper operation of the project: the test section is considered adiabatic; all the heater power is applied for the test fluid vaporization in the test section ($\dot{m}_{evap}$ in Fig. 2b), which is afterwards condensed on the internal surfaces of the pipeline and condenser; only film condensation takes place, whose heat transfer coefficients are lower than those observed for dropwise condensation; fully developed film condensation starts after one second, time during which an exponential function was used to represent a transition (see Section 2.3 for more details on the shape of the function); two uniform wall temperatures are considered, one for the pipeline (T_{wall_1}) and other for the condenser (T_{wall_2}); the walls initial temperatures are equal to the ambient temperature (20°C); a minimum value L_{min} is used when the condensing length, either for the pipeline or the condenser, is less than this critical value; the minimum value for the difference between the saturation and wall temperatures is dT_{min}.

The mass balance for the CV is:

$$\frac{dm_{CV}}{dt} = \dot{m}_{evap} - \dot{m}_c = \frac{\dot{q}_{heater}}{h_{fg}} - \frac{\dot{q}_{c_1} + \dot{q}_{c_2}}{h_{fg}} \tag{1}$$

where $\dot{q}_{heater}$ is the heater power (500 W), $\dot{q}_{c_1}$ is the heat flux related to condensation on the pipeline, $\dot{q}_{c_2}$ is the heat flux related to the condenser and h_{fg} is the fuel's heat of vaporization.

It follows that:

$$\frac{dL}{dt} = \frac{\left[\dot{q}_{heater} - f_{deg}\left(\dot{q}_{c_1} + \dot{q}_{c_2}\right)\right]}{\rho_v A_{cross} h_{fg}} \tag{2}$$

where f_{deg} is a degradation parameter better explained in Section 2.3, ρ_v is the vapor phase density and A_{cross} is the tube internal cross-sectional area.

The thermal-electrical analogy was considered to model the heat flux of condensation, which is dissipated by free convection with air for the pipeline and with water for the condenser. The conduction thermal resistances were neglected after performing some calculations that revealed a very small difference between the internal and external temperatures of the walls. The following iterative procedure was applied to model the transient phenomenon and estimate the wall temperatures:

$$T_{wall_k}(i) = T_{wall_k}(i-1) + dt\frac{q_{c_k}(i) - q_{fc_k}(i)}{m_{tube_k}(i)c_{p_{steel}}} \tag{3}$$

where k can be equal to 1 (pipeline) or 2 (condenser), m_{tube_k} are the associated steel masses, and $c_{p_{steel}}$ is the steel specific heat capacity.

2.2. Condensation and free convection correlations

The condensation heat fluxes can be represented by Newton's cooling law as follows:

$$q_{c_k} = \bar{h}_{c_k}\pi D_{tube,i}L_k(T_{sat} - T_{wall_k}) \tag{4}$$

With the intention of performing conservative calculations of the project variables, it was decided to disregard the initial drop-wise condensation and consider only film-wise condensation. Hence, the film condensation HTC ($\bar{h}_c$) was estimated with the laminar film condensation for vertical plates theory formulated by Nusselt (1916) [6].

For the free convection on the external surface of the condenser (inside the water jacket), we have:

$$q_{fc_k} = \bar{h}_{fc_k}\pi D_{tube,e}L_k(T_{wall_k} - T_{sat}) \tag{5}$$

The Churchill and Chu (1975) [7] correlation for free convection on vertical plates may be applied over the entire range of Ra_L and was used to estimate the free convection HTCs ($\bar{h}_{fc}$).

2.3. Characteristic times of boiling and condensation phenomena

The characteristic time of a physical phenomenon can be associated with the time interval required for its onset from the moment the conditions for its occurrence are established. Boiling and condensation are phenomena with considerably low characteristic times. For condensation of pure steam at atmospheric pressure, the onsetting process is ultimately instantaneous [8]. As one can see from the experimental study of Ma et al. (2010) [8] on the transient characteristics of droplet size and effect of pressure on evolution of transient condensation of water on a low thermal conductivity surface, as the pressure increases, there is a decreasing tendency for the time required for all the stages of drop-wise condensation to be completed. For ambient pressure, it is possible to assume that the stage I (nucleation stage) is completed after 0.5 s. Therefore, also considering that in our model condensation takes place on steel, whose conductivity is higher than that of polycarbonate, the time interval conservatively considered for the film condensation to fully establish is one second. This assumption is made with the interest of performing a conservative calculation of the phenomena that ensures the proper operation of the pressure control system.

Toward that direction, aiming to account for a delay between vapor entering the condenser and the film condensation settling, but also aiming to smooth the onset of the phenomenon, the following degradation function was used to transition the heat removed by condensation

between 0% ($t = 0\ s$) and 100% ($t = t_0 = 1\ s$) of that expected by the correlation of film-wise condensation.

$$f_{deg} = \frac{\exp \frac{t}{t_{deg}} - 1}{\exp \frac{t_0}{t_{deg}} - 1} \tag{6}$$

where t_{deg} is the shape parameter of the function.

Figure 6 shows how the shape of the function f_{deg} varies for different values of t_{deg}. Note that the smaller the value of t_{deg}, the closer to a step function f_{deg} becomes. The higher the value, the closer to a straight line.

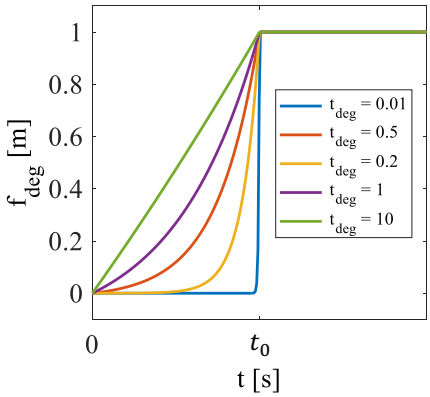

Figure 3: *Shape of the degradation function for different values of* t_{deg} *and* $t_0 = 1\ s$.

2.4. Pressure variation estimation

The initial condition of the system is taken to be the pre-compression of the spring towards the experiment pressure, when all the fluid is in the liquid phase and at room temperature. The pressure variation is estimated for each time interval (i) as follows:

$$dP_i = \frac{k_{spring} dx_i}{A_{piston}} \tag{7}$$

$$dx_i = \frac{V_{gas_{dL(i)}} - V_{liq_{dL(i)}}}{A_{piston}} \tag{8}$$

$$V_{gas_{dL(i)}} = \frac{\pi D_{int}^2}{4} dL(i) \tag{9}$$

where k_{spring} is the spring stiffness, dx_i is the piston and spring displacement, D_{int} is the pipeline and condenser tube internal diameter, $V_{gas_{dL(i)}}$ is the condensation volume variation at the time interval, $V_{liq_{dL(i)}}$ is the volume occupied by $V_{gas_{dL(i)}}$ when at ambient conditions and $dL(i)$ is the condensation length variation at the time interval estimated with Eq. 2.

3. Results and discussion

The variables of interest involved in the dimensioning of the spring-piston setups for the different pressure levels are the maximum force (F_{max}) and maximum displacement exerted on the spring (x_{max}), the maximum length of condensation (L_{max}), and the maximum pressure

reached during the experiments (P_{max}). To guide the selection of appropriate diameters for the pistons and spring stiffness coefficients, graphs were prepared to examine the behavior of these variables with varying piston diameter and for springs of different stiffness coefficients. A pressure tolerance parameter (α) was included to the pressure variation analysis:

$$\alpha = \frac{P_{max}}{P_0} \tag{10}$$

Therefore, accepting a tolerance of 20% variation of the test initial pressure ($\alpha = 1.2$), a straight line with value 1 can be drawn as an upper limit reference on the graph shown in Fig. 4a. In this context, the region of Fig. 4a below the black line consists of projects with less than 20% variation in initial pressure, and the region above corresponds to more than 20% variation in initial pressure. Furthermore, based on the analysis of spring manufacturers' catalogs, it is possible to use maximum project values $F_{p,max}$ (2200 N) and $x_{p,max}$ (90 mm) above which no springs are commercially available. This approach is adopted in the graphs of Fig. 4, that exemplifies the analysis for experiments at 10 bar with $t_{deg} = 0.3$ and $\alpha = 1.2$. For Figs. 4a, 4c and 4d, the regions of the graph with y-axis values smaller than 1 are considered as possible choices for the project variables, while Fig. 4b gives the maximum condensing length to be reached. For example, if $k_{spring} = 20$ N/mm, the piston diameter must be between 35 mm, limited by the pressure criterion, and 45 mm, given by the spring compression criterion. In this case the maximum condensing length is shorter than 0.38 m.

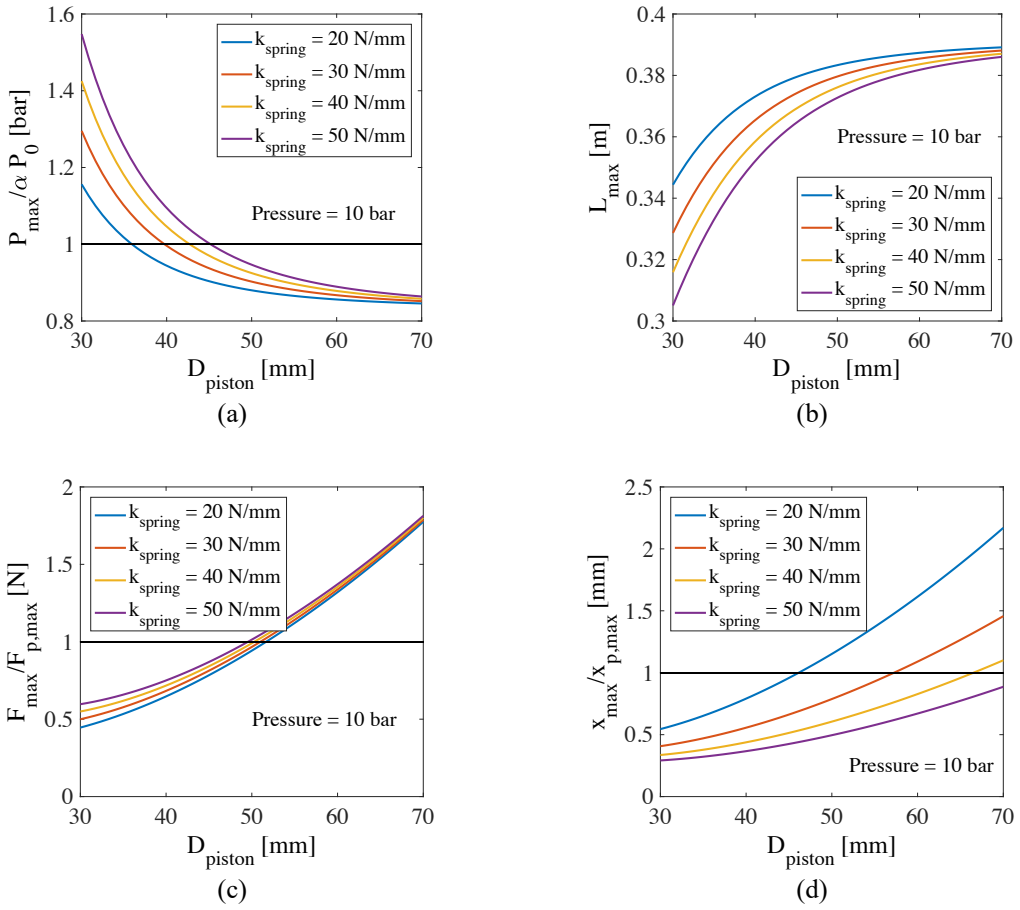

Figure 4: *Project variables analysis for tests at 10 bar.*

Based on this approach, Table 2 displays the selected feasible project values for the different pressure levels, while Table 3 shows springs A and B characteristics. We aimed to minimize the differences between the arrangements by using similar diameters and springs between them when possible.

Pressure [bar]	Piston diameter [mm]	Spring	Number of springs [-]
5	45	A	1
10	45	A	1
20	32	B	1
40	32	A	2
80	32	A	4

Table 2: *Spring-piston setups.*

Spring	Stiffness [N/mm]	Max. load [N]	Max. displac. [mm]
A	23.333	2100	92
.B	31.111	2260	76

Table 3: *Springs characteristics.*

Figure 5 shows the transient results obtained for the different pressure levels. The filled lines represent the analysis with $t_{deg} = 0.3$ while the dashed lines are the system response without considering the initial condensation degradation. We can see that the lower the pressure, the greater the required condensing length (Fig 5b), given that for lower pressures a greater density variation is observed between the liquid and vapor phases. At 8 seconds of simulation the heater is turned off. Therefore, we see a rapid drop in the graphs at this instant until $L = 0.2\ m$, when the condensed liquid fills the entire condenser tube, and then a slower drop for the fluid condensing in the pipeline exposed to air. It is possible to see that, even considering the initial degradation of the heat exchange, the system is nevertheless able to operate within the predefined project ranges. Considering Fig. 5b, and aiming for an oversized design, a 0.8 m condenser length is considered sufficient for the project.

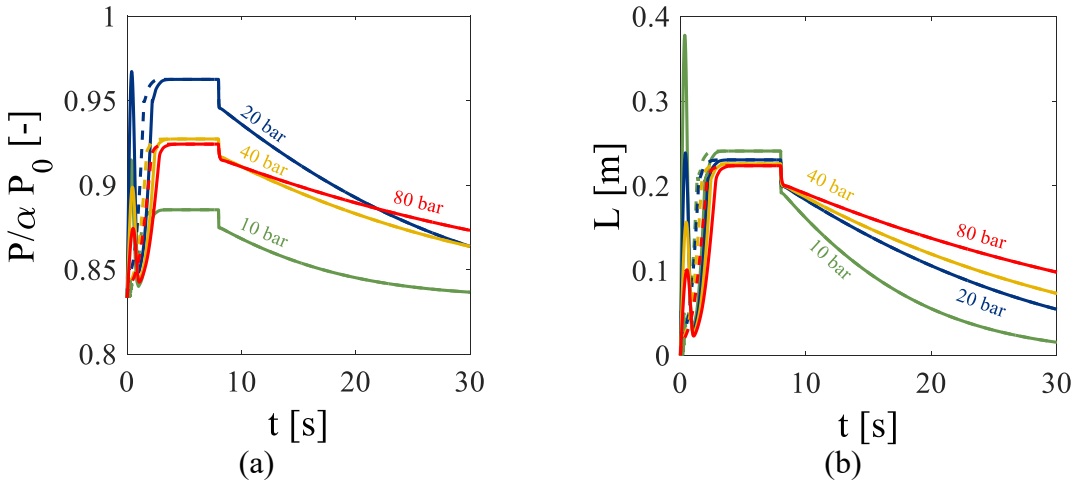

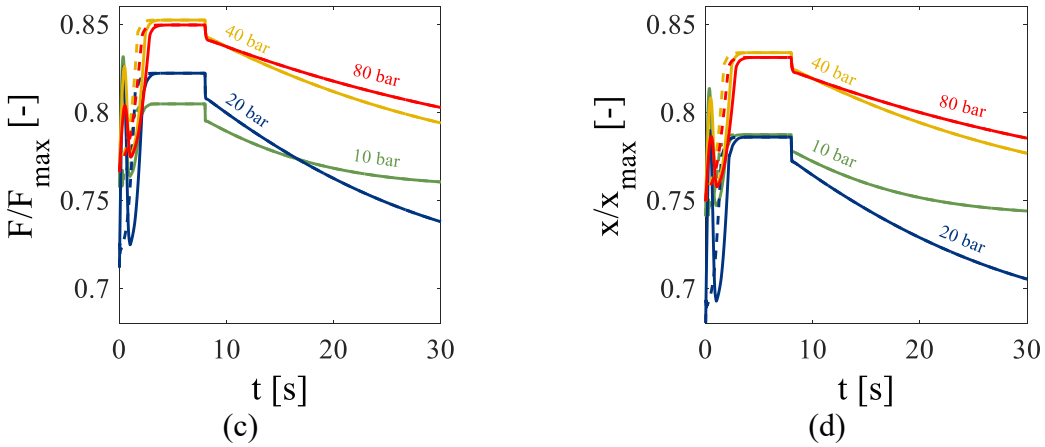

Figure 5: *Transient behavior of the project variables for different pressure levels. (a) pressure, (b) condensing length, (c) force acting on spring, and (d) spring displacement.*

4. Conclusion

In this paper the project of a test bench capable of operating at approximately constant pressure during fast pool boiling experiments was originally proposed. It includes a condenser and spring-piston assemblies. From its simulation and considering the operating characteristics of commercially available springs, the system could be conservatively dimensioned to perform the desired fast boiling experiments at pressures up to 80 bar.

References

[1] Huang, Y., Hong, G., Investigation of the effect of heated ethanol fuel on combustion and emissions of an ethanol direct injection plus gasoline port injection (EDI+ GPI) engine, *Energy Convers. Manag*., 123 (2016), 338-347.

[2] Schulz, F., Beyrau, F., The effect of operating parameters on the formation of fuel wall films as a basis for the reduction of engine particulate emissions, *Fuel*, 238 (2019), 375-384.

[3] Saliba, G., Saleh, R., Zhao, Y., Presto, A. A., Lambe, A. T., Frodin, B., ... Robinson, A. L., Comparison of gasoline direct-injection (GDI) and port fuel injection (PFI) vehicle emissions: emission certification standards, cold-start, secondary organic aerosol formation potential, and potential climate impacts, *Environ. Sci. Technol*., 51(11) (2017), 6542-6552.

[4] Du, B., Zhang, L., Geng, Y., Zhang, Y., Xu, H., Xiang, G., Testing and evaluation of cold-start emissions in a real driving emissions test, *Transp. Res. D: Transp. Environ.*, 86 (2020), 102447.

[5] Yusuf, A. A., Inambao, F. L., Effect of cold start emissions from gasoline-fueled engines of light-duty vehicles at low and high ambient temperatures: Recent trends. *Case Stud. Therm. Eng.*, 14 (2019), 100417.

[6] Nusselt, W., The surface condensation of water vapour. *Z VDI*, 60 (1916), 541-546.

[7] Churchill, S. W., Chu, H. H., Correlating equations for laminar and turbulent free convection from a vertical plate. *Int. J. Heat Mass Transf.*, 18(11) (1975), 1323-1329.

[8] Ma, X. H., Song, T. Y., Lan, Z., Bai, T., Transient characteristics of initial droplet size distribution and effect of pressure on evolution of transient condensation on low thermal conductivity surface. *Int. J. Therm. Sci.*, 49(9) (2010), 1517-1526.

Acknowledgements

This study was financed in part by LEMTA (Université de Lorraine), and by the Coordenação de aperfeiçoamento de Pessoal de Nível Superior – Brasil (CAPES) – Finance Code 001. We also thank the Brazilian federal program ROTA 2030 for the financial support of the construction of the test bench.